Label-free slot-waveguide biosensor for the detection of DNA hybridization

Tuffail Dar,[1,*] Jiri Homola,[2] B. M. Azizur Rahman,[3] and Muttukrishnan Rajarajan[4]

[1]School of Engineering and Mathematical Sciences, City University, Northampton Square, London EC1V 0HB, UK

[2]Department of Optical Sensors, Institute of Photonics and Electronics Prague, Room: I/14, Main building of IPE, Praha 8–Kobylisy, Chaberska. 57, Prague 182 51, Czech Republic

[3]School of Engineering and Mathematical sciences, City University London, Room: C166, Northampton Square, London EC1V 0HB, UK

[4]School of Engineering and Mathematical sciences, City University London, Room: C137, Northampton Square, London EC1V 0HB, UK

*Corresponding author: tuffaildar@gmail.com

Received 10 April 2012; revised 26 July 2012; accepted 27 August 2012; posted 26 October 2012 (Doc. ID 166452); published 30 November 2012

A finite element method based on the full-vectorial ***H***-field formulation has been employed to achieve the maximum field penetration in the sensing medium of the slot-waveguide-based ring resonator biosensor. The use of nanometer scale guiding structure where optical mode is confined in a low-index region permits a very compact sensor with high optical intensity in the region, which makes it possible to detect minimum refractive index change, and offers higher sensitivities. We analyze the change in effective refractive index of mode, sensitivity, and power confinement of the proposed slot-waveguide-based ring resonator biosensor for the detection of DNA hybridization. The biosensor exhibited theoretical sensitivity of 856 nm per refractive index unit (RIU) and a detection limit of 1.43×10^{-6} RIU. © 2012 Optical Society of America

OCIS codes: 130.6010, 160.1435, 280.1415, 280.1545, 280.4788, 230.5750.

1. Introduction

In the past decade, several types of biosensors were developed for applications in medicine, environmental monitoring, and homeland security. Label-based biosensors, such as fluorescence biosensors, require complex liquid handling and labelling procedures and a relatively long assay time. Hence, a label-free biosensor is an attractive alternative for future biosensing applications. Several groups developed different detection methods of label-free biosensors [1–6]. Label-free optical methods for detecting biological and chemical interactions have a number of advantages, such as the possibility to monitor biomolecular interaction in real time and detect analytes directly without the need for labelling. In particular, the slot waveguide biosensor is a useful device for monitoring the binding events between biomolecules in real time without the need for an intrinsic or extrinsic labels.

Slot waveguides present an interesting alternative when compared to rib- or strip-waveguide-based biosensors where light is predominantly guided in the high-index material. The light thus has little interaction with the biomaterial. This is a drawback for biosensing applications where small refractive index variations caused by biomolecular interactions are monitored. In the case of a slot waveguide, light is confined in a low-index slot region sandwiched between two high-index rails. Due to the discontinuity of the electric field at the interface between the rails

1559-128X/12/348195-08$15.00/0

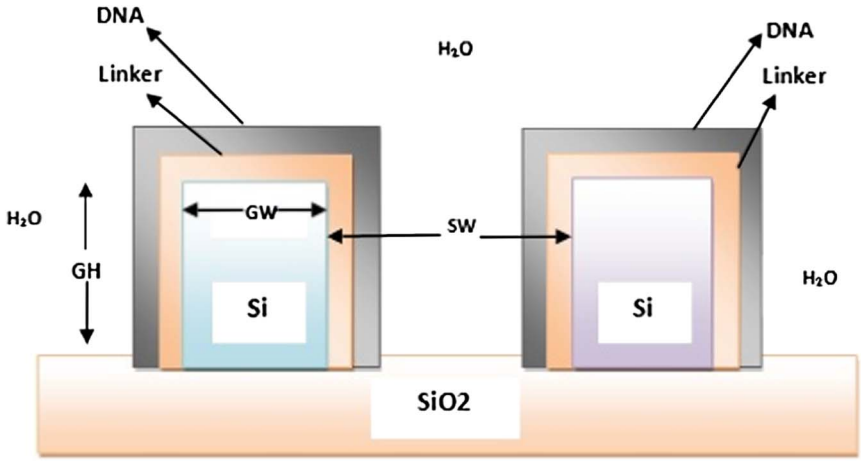

Fig. 1. (Color online) Slot waveguide biosensor.

and slot, a significant fraction of the electromagnetic field is localized in the slot.

The sensitivity of an optical waveguide sensor relies on the amount of light in the medium to be sensed. Due to the increased amount of power confined in the slot region, higher sensitivities will be achieved as compared to other waveguide-based biosensors.

This paper will investigate a slot-waveguide-based ring resonator biosensor using the finite-element-based numerical method for the detection of DNA hybridization, i.e., when single-stranded DNA (ssDNA) becomes double-stranded DNA (dsDNA). We assume that the ssDNA is initially immobilized on top of the linker layer (silanes) in the slot waveguide as the detection probe as shown in Fig. 1. When complementary DNA strands appear near the sensing surface with the immobilized probes, it will bind to the immobilized ssDNA probes forming dsDNA.

2. Theory

In the present work, the ***H***-field finite element method (FEM) based full-vector formulation is used for the solution of the TE and TM slot waveguide modes where the TE mode is highly confined in the slot region as compared to the TM mode. In the FEM, a problem domain can suitably be divided into a patchwork of a finite number of subregions called "elements." Each of the elements can have different shapes and sizes and by using many elements a complex problem can be accurately represented. In using the aforementioned approach, the field distribution in the transverse plane is obtained by the application of the variational formulation in the region. More recently, slot-waveguide-based biosensors have been investigated using the finite-difference time-domain method and the FEM [7–9].

A full-vectorial FEM is used in this study to obtain the modal solutions of a slot waveguide. The FEM, based on the vector-***H***-field formulation has been established as one of the most accurate and numerically efficient approaches to obtaining the modal field profiles and propagation constants of the fundamental and higher-order quasi-TE and TM modes. The full-vectorial formulation is based on the minimization of the following functional in terms of the nodal values of the full ***H***-field vector:

$$\omega^2 = \frac{\int [(\nabla \times H)^* \cdot \varepsilon^{-1} (\nabla \times H) + p(\nabla \cdot H)^* (\nabla \cdot H)] \mathrm{d}x\mathrm{d}y}{\int H^* \cdot \mu H \mathrm{d}x\mathrm{d}y}, \tag{1}$$

where ***H*** is the full vectorial magnetic field, $*$ denotes a complex conjugate and transpose, ω^2 is the eigenvalue where ω is the angular frequency of the wave, and ε and μ are the permittivity and permeability, respectively.

In the present work, by optimizing the slot waveguide parameters such as the slot width, guide width, and guide height a compact biosensor is proposed. The aim of the paper is to provide a novel comprehensive analysis defining the modal characteristics, effective index variation of ssDNA and dsDNA, surface sensitivity, and power confinement in the DNA layer of a slot waveguide biosensor with a nanoscale cross section, and in doing so, the effects of the critical size of such a waveguide are also presented. To undertake such analysis, an accurate and numerically efficient vector-***H***-field finite element method (VFEM) [10] is used to calculate the propagation constant, effective index, power confinement factor, and the full-vectorial modal field profiles of the waveguide. The full-vectorial electric field (***E***) is also derived from the vector ***H***-field obtained to characterize modal properties of such waveguides.

3. Results

A. Waveguide Structure

In this paper, a slot waveguide is investigated for the biosensing applications. A slot waveguide is formed by two Si wires close to each other having nanometer dimensions, as shown in Fig. 1. Refractive index (RI) of silicon, silicon oxide, and water is taken as 3.476, 1.444, and 1.31, respectively, at the operating wavelength of 1550 nm. The sensing structure is first

coated with a linker layer (silanes) whose refractive index is taken as 1.42 [11] having a thickness of $t = 1$ nm. The actual sensing consists of detection of the complementary DNA sequence. The refractive index of ssDNA and dsDNA is taken as 1.456 and 1.53 [12], respectively. The thickness of the DNA probe layer is taken as $n = 8$ nm and remains unchanged when binding of complementary DNA strands (targets) to DNA probes happens, i.e., only refractive index changes from 1.456 (ssDNA) to 1.53 (dsDNA).

A waveguide height, GH = 320 nm and high index region width, GW = 180 nm [7], slot width, SW = 100 nm, linker layer thickness of $t = 1$ nm, and DNA probe thickness of $n = 8$ nm is considered for the initial simulation study.

B. Modal Solutions

In the study of modal field profile, the ***H***-field-based VFEM is used to obtain the modal solutions of such a waveguide. For this study, due to the availability of twofold symmetry of the waveguide structure, only a half of the structure is considered, in which more than 80,000 irregular-sized first-order triangular elements have been employed to represent the waveguide structure. It takes about 2 min cpu time on a dual-core Pentium processor computer running solaris platform.

The structure supports both fundamental quasi-TE and quasi-TM modes. For the quasi-TE mode the H_y field component is dominant, and H_x and H_z are the nondominant components. The dominant H_y field component of the H_y11 mode is shown in Fig. 2 for the waveguide width, GW = 180 nm, and height, GH = 320 nm.

In its contour plot, as shown in Fig. 3, it is clearly visible that the modal confinement is much stronger in the slot region. Due to the large index contrast at interfaces, the normal electric field undergoes a large discontinuity, which results in a field enhancement in the slot region.

C. Effective Index Variation

The variation in the effective index of the fundamental H_y11 mode for a slot waveguide has been studied.

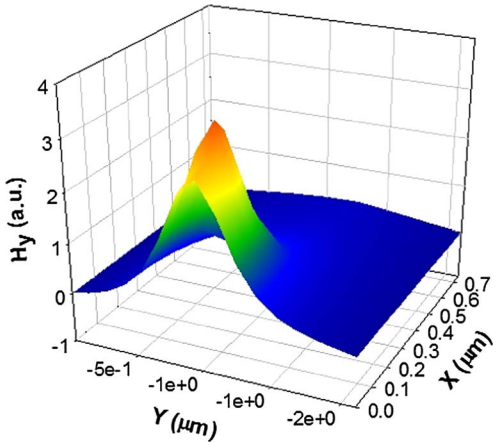

Fig. 2. (Color online) H_y field of the H_y11 mode.

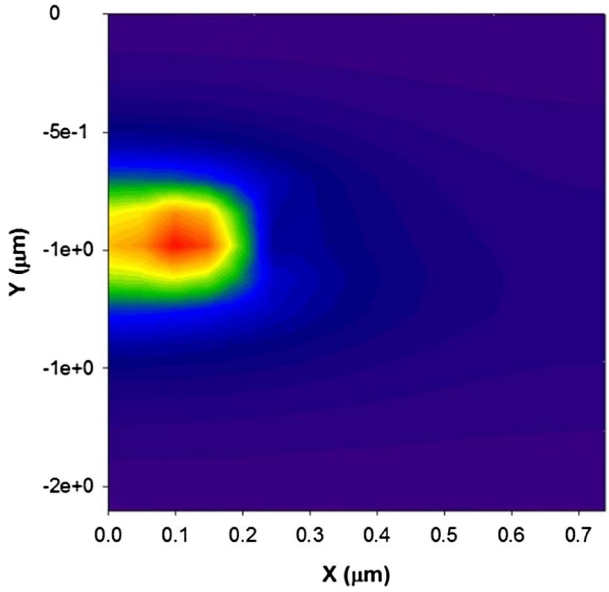

Fig. 3. (Color online) H_y contour of H_y11 mode.

The effective index, n_{eff}, of a given mode is a normalized propagation parameter, which can be defined by $n_{\text{eff}} = \beta_0/k_0$, where β_0 is the propagation constant of that mode and k_0 is the free space wavenumber defined as $k_0 = \omega(\varepsilon_0\mu_0)^{1/2} = 2\pi/\lambda$. The various simulations are carried out to yield the maximum effective index difference so that maximum waveguide sensitivity is achieved and small size compact biosensor is designed.

For biosensing applications effective index change is an important design parameter. In Fig. 4 variations of the effective index (n_{eff}) with the slot width for the fundamental H_y11 mode is presented. A waveguide height, GH = 320 nm, and high index region width and GW = 180 nm is considered for the study of simulations. In Fig. 4, the solid line represents the water as the sensing medium, the dotted line represents the linker layer (thickness $t =$ 1 nm and RI = 1.42), and water as the sensing

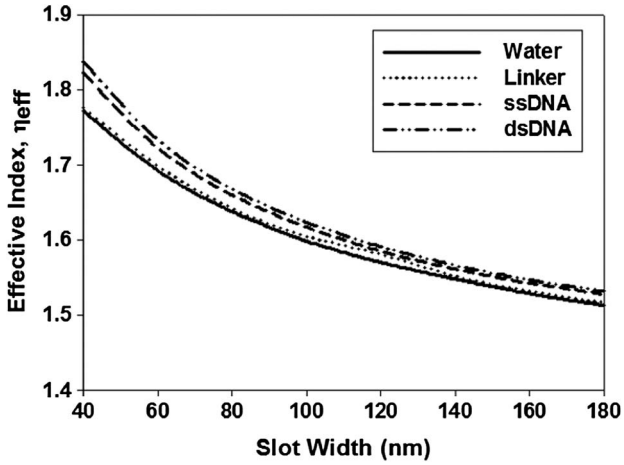

Fig. 4. Variations of the effective index, n_{eff}, with the slot width for TE mode.

layers; the dashed line represents the linker layer, ssDNA (thickness $n = 8$ nm and RI $= 1.456$), and water as the sensing layers; and the dashed-dotted line represents the linker layer, dsDNA (thickness $n = 8$ nm and RI $= 1.53$), and water as the sensing layers. In all the cases it shows the effective index decreases with the increase in slot width because when the slot gap is small a stronger coupling occurs and hence increases the effective index. It is also shown that the effective index is higher when the sensing medium is dsDNA, as represented by dashed-dotted line in Fig. 4.

D. Sensitivity

In sensor development, sensitivity is an important parameter to evaluate the sensor performance. Fundamentally, sensitivity is determined by the strength of light–matter interaction. For an optical label-free sensor, sensitivity can be divided into waveguide sensitivity and device sensitivity. Device sensitivity is defined as the ratio of the change in the transducing optical parameter to the effective index change, while waveguide sensitivity is the ratio of the effective index change to the change in the waveguide parameter affected by analytes.

1. *Waveguide Sensitivity*

The effective index change is produced either by a change of cover medium refractive index (homogeneous sensing) or by a change of thickness of DNA layer, which is immobilized on waveguide surface (surface sensing) [8]. Measurement sensitivity depends on optical field distribution in the sensing medium, so one of the most important design tasks is the waveguide optimization in order to maximize its sensitivity.

Adlayer thickness and change of cover medium refractive index affects the effective index of propagating optical mode. The thickness of the DNA probe layer is taken as 8 nm and remains unchanged when binding of complementary DNA strands (targets) to DNA probes happens and the refractive index of ssDNA and dsDNA is taken as 1.456 and 1.53, respectively.

Waveguide sensitivity can be written as

$$S = \delta n_{\text{eff}}/\text{RI}, \tag{2}$$

where RI is the DNA layer refractive index and δn_{eff} is the effective index difference when ssDNA and dsDNA are present. The effective index difference is achieved by simulating first by adding ssDNA layer on top of linker layer and then replacing ssDNA by dsDNA layer.

A waveguide height, GH $= 320$ nm, is fixed and SW $= 60$, 100, and 140 nm is varied. The sensing layers are the linker layer (thickness $t = 1$ nm and RI $= 1.42$), ssDNA (thickness $n = 8$ nm and RI $= 1.456$), and water, respectively. We have then replaced the ssDNA layer with the dsDNA (thickness $n = 8$ nm and RI $= 1.53$) to achieve the difference between the two.

Figure 5 shows that larger effective index variation and waveguide sensitivity is achieved at a guide width $= 220$ nm when the slot width is 60, 100, and 140 nm, respectively. The greater the change in δn_{eff} the more sensitive the biosensor will be. Therefore, when the guide width is between 200 and 220 nm, maximum index difference is achieved. Although, a smaller slot width shows a more sensitive design, considering the fabrication techniques available today, a 100 nm slot width would be a suitable design.

Figure 6 shows that the change in effective index and waveguide sensitivity decreases with the increase in the slot width due to the presence of DNA layers. A waveguide height, GH $= 320$ nm, is fixed and GW $= 140$, 180, and 220 nm, is varied. The sensing layers are the linker layer (thickness $t =$ 1 nm and RI $= 1.42$), ssDNA (thickness $n = 8$ nm and RI $= 1.456$), and water, respectively. We have replaced the ssDNA layer with the dsDNA (thickness $n = 8$ nm and RI $= 1.53$) to achieve the difference between the two. A large effective index variation is achieved when the slot width is less than 100 in all cases. Although, a smaller slot width shows a more sensitive design, considering the fabrication techniques available today, a 100 nm slot width would be a suitable design.

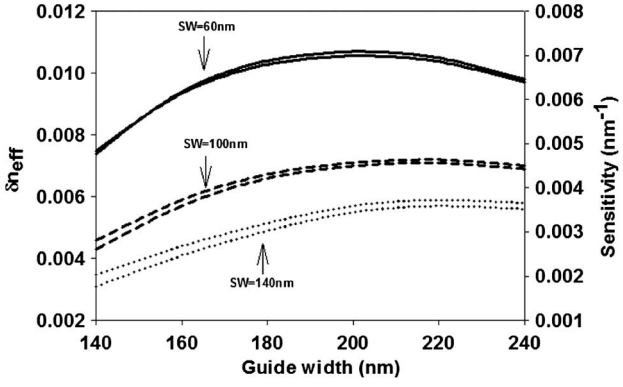

Fig. 5. Variation of effective index difference, δn_{eff} and waveguide sensitivity with guide width.

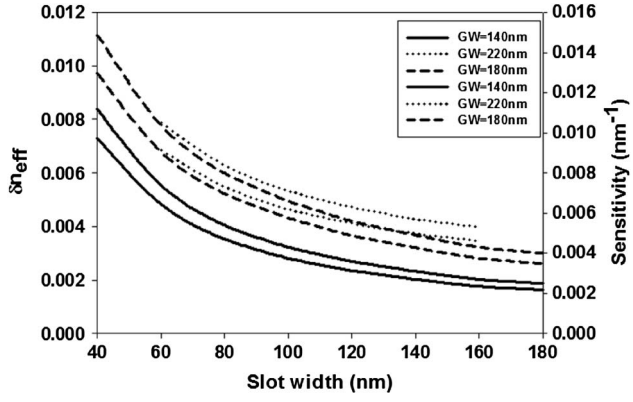

Fig. 6. Variation of effective index difference, δn_{eff} and waveguide sensitivity with slot width.

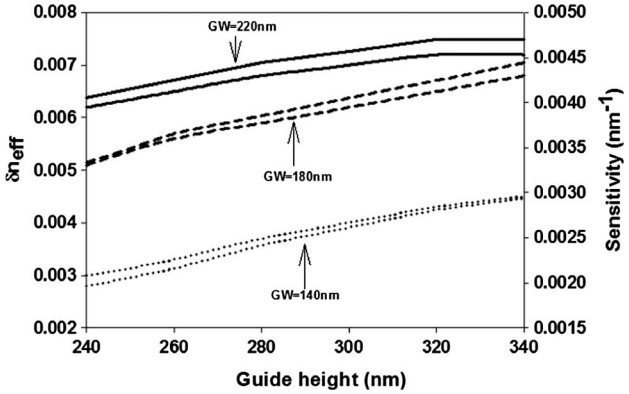

Fig. 7. Variation of effective index difference, δn_{eff} and waveguide sensitivity with guide height.

Figure 7 shows variation of effective index difference and waveguide sensitivity with the guide height. When the guide width is between 180 and 220 nm and slot width is 100 nm, the maximum effective index difference can be achieved as compared to a guide width 140 nm. The effective index difference increases with the increase in guide height. However, if the waveguide dimension becomes too large, most of the power would be then confined in the Si core and a smaller effective index difference can be achieved, hence less sensitivity and less confinement in the slot region. A line needs to be drawn to achieve a compact and smaller biosensor, therefore guide heights between 320 and 340 nm are the desirable dimensions.

2. *Device Sensitivity*

We present a ring resonator comprised of a silicon on insulator (SOI) slot waveguide for the detection of DNA hybridization. In our case, to achieve the theoretical device sensitivities we are using the same parameters of ring as is used in [12], including 5 μm of bending radius.

Device sensitivity only depends on device properties, and waveguide sensitivity is relevant to waveguide structures, regardless of the type of devices. Based on the definition, device sensitivity is related to the variation of transducing optical parameters, and thus depends on the transducing method. For the resonant wavelength shift scheme, it is expressed as

$$S = \delta\lambda/\delta n, \tag{3}$$

$$\delta\lambda = \delta n_{\text{eff}} * \lambda_{\text{res}}/n_g, \tag{4}$$

where δn_{eff} is the change of the effective index caused by the analyte binding, λ_{res} is the resonance wavelength, and n_g is the group index and its value is 1.81264 at wavelength of 1550 nm, as shown in Fig. 8, when silicon width is 220 nm, height is 320 nm, and slot width is 100 nm.

As a function of slot width and guide width, the effective index of the waveguide was simulated once for ssDNA and once for dsDNA. By using Eq. (4), the difference in effective index $\delta n_{\text{eff}} = n_{\text{eff,ssDNA}} - n_{\text{eff,dsDNA}}$ was used to calculate the expected wavelength shift of the slot waveguide.

Figures 9 and 10 show the calculated resonance wavelength shift as a function of slot width and guide width. In this range of the parameters, the sensitivity increases with decreasing the slot width. When silicon width is 220 nm, height is 320 nm, and slot width is 100 nm our simulation shows that effective refractive indices of ssDNA and dsDNA are 1.80549 and 1.81264, respectively, 6.12 nm resonance wavelength shift, and sensitivity of 856 nm/RIU is achieved.

When compared with [12] where sensitivity of 683 nm RIU^{-1} is achieved for the detection of DNA hybridization with slot width of 200 nm and guide width of 500 nm. In our sensor, a large resonance wavelength shift is caused by large light–matter interaction and by decreasing the slot width.

A comparison is made with the following structures: [13,14] and [12], respectively. In case of [13] where slot width = 100 nm, guide width = 210 nm, guide height = 220 nm, RI = 1.45, and a wavelength shift is 5.4 nm. When the same parameters are simulated using our method, a wavelength shift of 5.56 nm is achieved. Similarly, in case of [14],

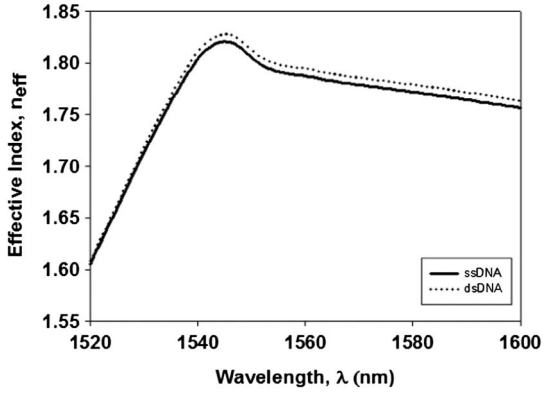

Fig. 8. Variation of effective index with wavelength.

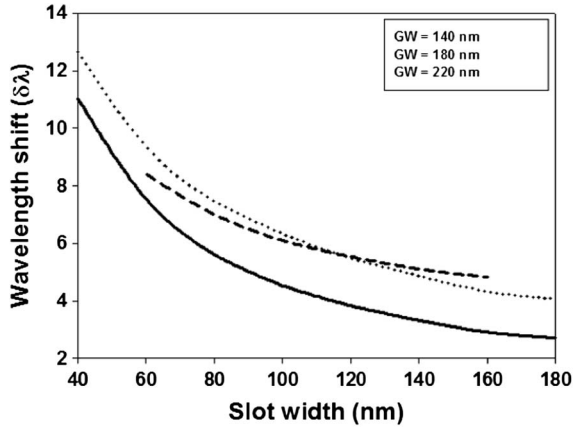

Fig. 9. Variation of wavelength shift with slot width.

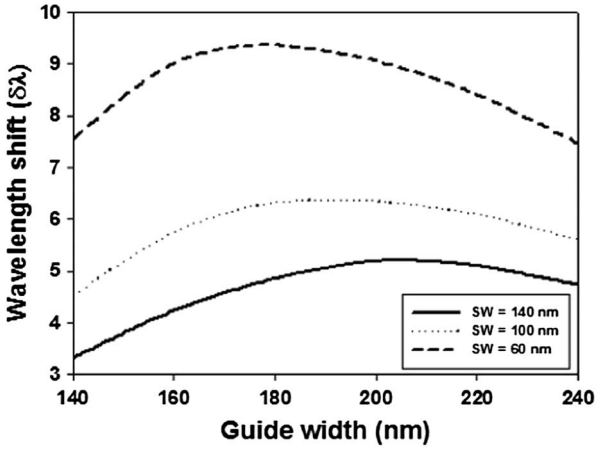

Fig. 10. Variation of wavelength shift with guide width.

where slot width = 200 nm, guide width = 400 nm, guide height = 300 nm, RI = 1.45, and a wavelength shift is 3 nm. A wavelength shift of 3.2 nm is achieved in our simulations when using the same values of slot waveguide as in [14]. The same results of wavelength shift are achieved when the same slot waveguide parameters as in case of [12] are used (slot width = 200 nm, guide width = 500 nm, RI of ssDNA = 1.456, RI of dsDNA = 1.53, and a wavelength shift of 3.634 nm). This shows our numerical method is in agreement with the wavelength shift results in [12,13,14].

In [15], a similar waveguide is measured to have 12 dB/cm propagation loss due to scattering. As the absorption of water at a wavelength of 1.55 μm is 47.5 dB/cm [16], and our simulations indicate that 30% of the waveguide mode power propagates through water, we can roughly estimate the total propagation loss of our waveguide to be 12 dB/cm+ $0.3 * 47.5$ dB/cm = 26.25 dB/cm.

3. *Sensor Detection Limit*

Sensor detection limit (DL) is another important parameter to characterize the sensor performance. DL is the smallest change in the refractive index, which is equal to the resonance wavelength resolution divided by the sensitivity [13]. The DL can be deduced by taking into account the noise in the transduction signal, σ, i.e., the minimum resolvable signal: DL = σ/S, where S is the sensitivity. For an optical RI-based label-free sensor, DL in units of refractive index units (RIU) is naturally used to quantify the sensor performance, which enables a rough comparison of the sensing capability among different optical technologies and structures. [17]. We follow the convention of using 3 standard deviations σ of the total system noise as a measure of the sensor resolution [18]:

$$R = 3\sigma = 1.2 \text{ pm}. \tag{5}$$

Improvement in the DL can be accomplished by increasing the sensitivity or reducing the noise level. Sensitivity can be enhanced by increasing the light–matter interaction. For our sensor, the detection limit is 1.43×10^{-6} RIU.

E. Power Confinement

The confinement factor in any particular area normalized to the total power, which is obtained by integrating the Poynting vector, from the $\boldsymbol{H}$- and $\boldsymbol{E}$-fields is given below:

$$S_z = \iint_{\Omega} \{\boldsymbol{E} \times \boldsymbol{H}\} \mathrm{d}x\mathrm{d}y. \tag{6}$$

The waveguide sensitivity depends on the optical field confinement factor in the sensing medium. Quasi-TE mode supported by a slot waveguide is highly confined in the gap region and its confinement factor in the DNA layer is typically around 10%–12%, which means a very large sensitivity to cover index change. Quasi-TM mode is significantly less sensitive to cover index change and its confinement factor is only around 4%–5%.

As shown in Figs. 11(a) and 11(b), the difference in the field confinement between ssDNA and dsDNA is small and that is why the curves are plotted separately, otherwise they overlap with each other.

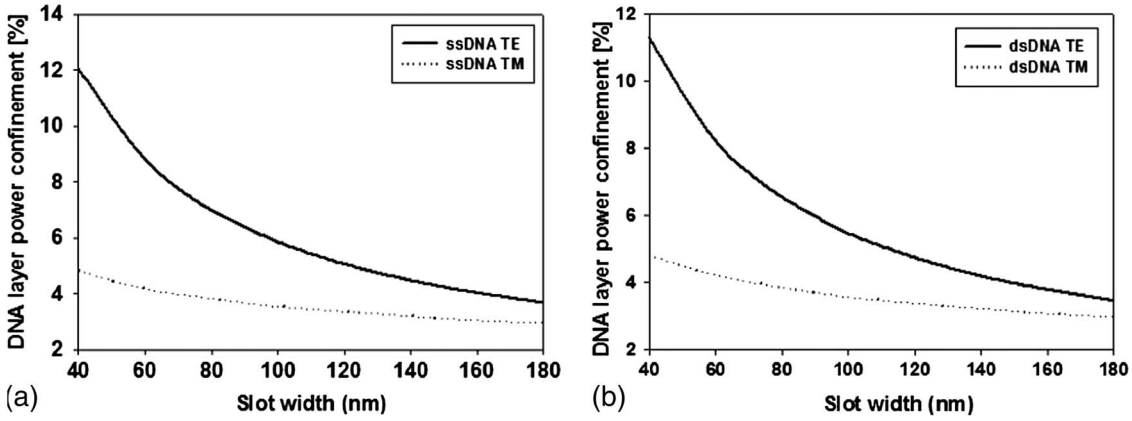

Fig. 11. Power confinement factor in (a) ssDNA layer and (b) dsDNA layer.

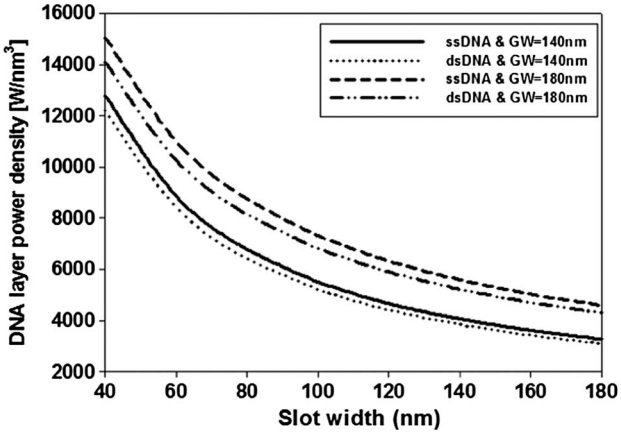

Fig. 12. Variation of power density in DNA layer with the slot width for TE mode.

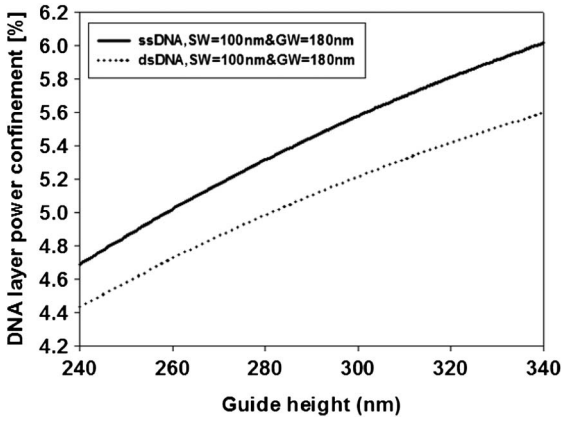

Fig. 14. Variation of power density in DNA layer with the guide height for TE mode.

TE mode has more power confinement because the normal electric field undergoes a large discontinuity, which results in a field enhancement in the slot region when the slot width is smaller. However, TM mode has less power confinement in the slot region because optical power is localized more in the high-index region and less confined in the slot region.

The slot width is varied from 40 to 180 nm keeping guide width as 220 nm and guide height as 320 nm. The highest power confinement is achieved when slot width is 40 nm and sensing medium is ssDNA. When the slot gap is smaller, stronger coupling occurs and hence more power confinement. However, it is important to remember the fabrication limitations that the slot width be less than 100 nm are not easy to fabricate and hence slot width of 100 nm is the minimum desirable width for the design of our biosensor.

Another important parameter in the design of such biosensors is the slot power density, which is defined as the power confinement in the sensing medium divided by the sensing medium area [9]. Figure 12 shows the variation of the slot power density for different slot widths keeping constant guide width of 140 and 180 nm, respectively, and guide height of 320 nm. The guide width of 140 and 180 nm is compared in order to achieve better results. The power density is a maximum when the slot width is smaller and the guide width is 180 nm. The smaller the slot widths the better the coupling efficiency. Power density is higher when the sensing medium is ssDNA as compared to dsDNA in both the cases of guide widths. When the index contrast is high the normal electric field undergoes a large discontinuity, which results in a field enhancement in the slot region; therefore, more power confinement in the slot region in case of ssDNA as compared with dsDNA.

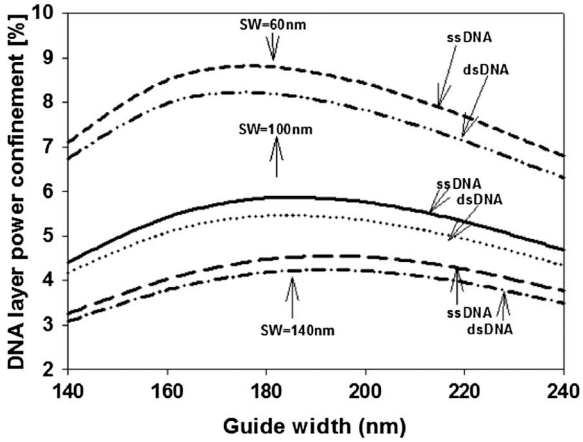

Fig. 13. Variation of power density in DNA layer with the guide width for TE mode.

Next, the effect of power confinement is measured by varying the guide width and keeping the sloth widths as 60, 100, and 140 nm, and guide height as 320 nm. The maximum power confinement is achieved when the guide width is 180 nm and the slot width is 60 nm, as shown in Fig. 13. Then followed by guide width of 180 nm and slot width of 100 nm. However, a slot width of 60 nm is not easy to fabricate; therefore, slot width of 100 nm and guide width of 180 nm is an ideal combination for achieving maximum power confinement. Again, it is evident that power confinement is higher when the sensing medium is ssDNA as compared to dsDNA in all the cases of varying slot widths due to its high-index contrast with the guide.

Further, the guide height is varied while keeping the slot width as 100 nm and guide width as 180 nm, which is the best possible combination, as shown above in Figs. 5 and 6. The power confinement increases with the increase in guide height, as shown in Fig. 14. As the waveguide dimension becomes large, most of the power would be confined in the Si core; however, due to restrictions in guide width and slot width we see power confinement in the DNA layer increases with the guide height. Most of the easily available wafers are of $H = 220$ nm, and slot waveguide of other heights needs to be fabricated specifically.

Comparing Figs. 12–14 with Figs. 5–7 it appears power confinement and sensitivity can be achieved with the same design parameters; where sensitivity

is maximum we can also see power confinement is maximum in all the cases.

4. Conclusion

A finite element approach based on a full-vectorial ***H***-field formulation has been used to study the slot waveguide biosensor to detect the DNA hybridization. The optical field profiles, the effective index change, power confinement factor, and power density in the DNA layer have been studied and an optimized slot waveguide sensor with maximum sensitivity is proposed. In this work we have proposed a method to detect DNA hybridization. When the complementary strand DNA attaches with the probe DNA, we see a change in the effective index and power confinement.

By taking the fabrication limitation into consideration slot width of 100 nm is a minimum desirable width for the design of a biosensor. Moreover, guide width of 180 to 220 nm and guide height of 320 nm gives us the compact and smaller size biosensor with maximum waveguide sensitivity, maximum effective index difference, and maximum power confinement factor in the DNA layer.

References

1. B. J. Luff, R. D. Harris, J. S. Wilkinson, R. Wilson, and D. J. Schiffrin, "Integrated-optical directional coupler biosensor," Opt. Lett. **21**, 618–620 (1996).
2. F. Prieto, B. Sepulveda, A. Calle, A. Llobera, C. Domynguez, A. Abad, A. Montoya, and L. M. Lechuga, "An integrated optical interferometric nanodevice based on silicon technology for biosensor applications," Nanotechnology **14**, 907–912 (2003).
3. W. C. L. Hopman, P. Pottier, D. Yudistira, J. van Lith, P. V. Lambeck, R. M. De La Rue, and A. Driessen, "Quasi-one-dimensional photonic crystal as a compact building-block for refractometric optical sensors," IEEE J. Sel. Top. Quantum Electron. **11**, 11–16 (2005).
4. C. Y. Chao, W. Fung, and L. J. Guo, "Polymer microring resonators for biochemical sensing applications," IEEE J. Sel. Top. Quantum Electron. **12**, 134–142 (2006).
5. R. I. W. Osmond, W. C. Kett, S. E. Skett, and E. R. Coombe, "Protein heparin interactions measured by BIAcore 2000 are affected by the method of heparin immobilization," Anal. Biochem. **310**, 199–207 (2002).
6. N. Nath and A. Chilkoti, "Label-free biosensing by surface plasmon of nanoparticles on glass: optimization of nanoparticles size," Anal. Chem. **76**, 5370–5378 (2004).
7. V. M. N. Passaro, F. Dell'Olio, C. Ciminelli, and M. N. Armenise, "Efficient chemical sensing by coupled slot SOI waveguides," Sens. Actuators B Chem. **150**, 417–424 (2010).
8. F. Dell'Olio and V. M. N. Passaro, "Optical sensing by optimized silicon slot waveguides," Opt. Express **15**, 4977–4993 (2007).
9. K. R. Hiremath, "Analytical modal analysis of bent slot waveguides," J. Opt. Soc. Am. A **26**, 2321–2326 (2009).
10. B. M. A. Rahman and J. B. Davies, "Finite element solution of integrated optical waveguides," J. Lightwave Technol. **2**, 682–688 (1984).
11. M. D. Malinsky, K. L. Kelly, G. C. Schatz, and R. P. Van Duyne, "Chain length dependence and sensing capabilities of the localized surface plasmon resonance of silver nanoparticles chemically modified with alkanethiol self-assembled monolayers," J. Am. Chem. Soc. **123**, 1471–1482 (2001).
12. X. Li, Z. Zhang, S. Qin, T. Wang, F. Liu, M. Qiu, and Y. Su, "Sensitive label-free and compact biosensor based on concentric silicon-on-insulator microring resonators," Appl. Opt. **48**, F90–F94 (2009).
13. T. Claes, J. G. Molera, K. De Vos, E. Schacht, R. Baets, and P. Bienstman, "Label-free biosensing with a slot waveguide based ring resonator in silicon on insulator," IEEE Photonics J. **1**, 197–204 (2009).
14. C. A. Barrios, M. J. Banuls, V. Gonzalez-Pedro, K. B. Gylfason, B. Sanchez, A. Griol, A. Maquieira, H. Sohlstrom, M. Holgado, and R. Casquel, "Label-free optical biosensing with slot-waveguides," Opt. Lett. **33**, 708–710 (2008).
15. C. Koos, P. Vorreau, T. Vallaitis, P. Dumon, W. Bogaerts, R. Baets, B. Esembeson, I. Biaggio, T. Michinobu, F. Diederich, W. Freude, and J. Leuthold, "All-optical high-speed signal processing with silicon-organic hybrid slot waveguides," Nat. Photonics **3**, 216–219 (2009).
16. K. Palmer and D. Williams, "Optical properties of water in the near infrared," J. Opt. Soc. Am. **64**, 1107–1110 (1974).
17. X. Fan, I. M. White, S. I. Shopova, H. Zhu, J. D. Suter, and Y. Sun, "Sensitive optical biosensors for unlabeled targets: A review," Anal. Chim. Acta **620**, 8–26 (2008).
18. C. F. Carlborg, K. B. Gylfason, A. Kazmierczak, F. Dortu, M. J. Banuls Polo, A. M. Catala, G. M. Kresbach, H. Sohlstrom, T. Moh, L. Vivien, J. Popplewell, G. Ronan, C. A. Barrios, G. Stemme, and W. van der Wijngaart, "A packaged optical slot-waveguide ring resonator sensor array for multiplex label-free assays in labs-on-chips," Lab Chip **10**, 281–290 (2010).